Atmos. Chem. Phys. Discuss., 15, 15977–16017, 2015
www.atmos-chem-phys-discuss.net/15/15977/2015/
doi:10.5194/acpd-15-15977-2015

Atmospheric Chemistry and Physics Discussions

Tropical, oceanic, deep convective cloud morphology as observed by CloudSat

M. R. Igel and S. C. van den Heever

Department of Atmospheric Science, Colorado State University, Fort Collins, CO, USA

Received: 7 April 2015 – Accepted: 24 May 2015 – Published: 12 June 2015

Correspondence to: M. R. Igel (migel@rsmas.miami.edu)

Published by Copernicus Publications on behalf of the European Geosciences Union.

Abstract

An investigation into the physical shape and size of mature, oceanic, tropical, deep convective clouds is conducted. A previously developed CloudSat data-partitioning methodology is used that separates components of cloud objects and measures their various length scales. In particular, the cloud objects are divided into a lower "pedestal" region on which the upper-level "anvil" region sits. Mean cloud objects are discussed in the framework of this morphological partitioning. For single-core clouds, the mean cloud has an anvil width of 95 km, a pedestal width of 11 km, and an anvil thickness of 6.4 km. The number of identified convective cores within the pedestal correlates positively with certain cloud length scales and morphological attributes of cloud objects such as anvil width. As the number of cores increases, the width of cloud objects is observed to grow. Pedestal width is shown to regress linearly to anvil width when a 2/3rd power scaling is applied to pedestal width. This result implies a decrease in the anvil width to pedestal width ratio with growing pedestals and an equivalence between the mass convected through the pedestal top and that into the anvil. Taller clouds are found to be wider. Some of the results obtained using the CloudSat methodology are also examined with a large-domain radiative-convective equilibrium numerical simulation and are found to exhibit similar trends when modeled. Finally, various CloudSat sampling issues are discussed in several appendices.

1 Introduction and background

Much of the basic study of deep convective cloud scales in the tropics has focused on squall lines and clusters (see Houze and Betts, 1981; Chen et al., 1996; Mohr and Zipser, 1996; Liu and Zipser, 2013) – the events that produce the majority of rainfall and have the greatest impacts on communities but which happen much less frequently than more benign, ordinary deep convection. Tropical meteorology is primarily composed of unremarkable oceanic, deep convection, which is only unremarkable because of its

high frequency. Riehl and Malkus (1958) famously recognized this more than 50 years ago, but it has not been until recently with the launching of various high-resolution satellites that the study of a large number of deep convective clouds over a long time period has become possible.

In a previous paper, Igel et al. (2014) suggested that examining the length scales of convective elements was both a novel and instructive endeavor. They discussed how these length scales of convection related to the climate impacts of deep, tropical, oceanic convection by examining trends in convective scales with respect to sea surface temperature (SST). Herein, the entire population of deep convective clouds will be treated equally because the objective of this paper is to quantify convective cloud scales in an effort to elucidate internal aspects of the nature of all convection. Thus, the paper will have two main themes. The first is to assess various convective scales and their interrelationships. The second is to use these interrelationships to shed light on convective dynamics. At the behest of Mapes (1997), it will be stated explicitly, that "scales" is used throughout this paper to mean "physical dimension".

Several investigations of convective scales occurred in the early days of the study of tropical convection. Between the landmark field campaigns of the Global Atmospheric Research Program (GARP) Atlantic Tropical Experiment (GATE) (National Academy of Sciences, 1971) and Tropical Ocean Global Atmosphere Coupled Ocean-Atmosphere Response Experiment (TOGA-COARE) (Webster and Lukas, 1992) as well as later in KWAJEX (Yuter et al., 2005) and earlier (Malkus and Riehl, 1964; Holle, 1968; Lopez, 1976), much was determined about the size and shape of tropical convection (Houze and Cheng, 1977; Houze 1982; Rickenbach and Rutledge, 1997; Johnson et al., 1999; Cetrone and Houze, 2006). This was achieved primarily through photogrammetric and radar analysis. What these local area studies and larger campaigns lacked fundamentally, though, was broad spatial and temporal coverage. Even when combined, GATE and TOGA-COARE covered less than 1 % of the global tropics. These works also tended to focus on the entire population of cumulus convection from shallow to deep cloud systems. Analyzing data with this focus rightfully points out the importance

of shallow convection to the entire population but fails to adequately detail the characteristics of deep convection given its comparative infrequence (Wood and Field, 2011). Other studies have tended to focus on the scales of various tropical mesoscale convective systems (MCS). While such systems can greatly impact communities due to their intensity, they only make up a small portion of the cloud population. The research presented here will focus on cataloguing the length scales of tropical deep convection that occurs up scale of frequent, trade wind convection and down scale of synoptic clusters of convection. That being said, MCSs are not excluded from the dataset. The clouds composing the dataset occur over all tropical oceans during the first 5 years of the CloudSat mission, 2006–2011. As in Igel et al. (2014), a cloud object approach will be used. This kind of technique has been utilized recently in a number of ways (e.g. Nesbitt et al., 2006; Bacmeister and Stephens, 2011; Riley et al., 2011; Dias et al., 2012). The goal behind using such a technique is to isolate individual clouds from the larger-scale environmental meteorology. It also allows for thorough statistical analysis by combining information from many individual clouds. The strength of the statistics provides for a variety of quantities to be treated as both independent and dependent variables through this paper.

Some of the first measurements of cloud sizes came out of GATE and were of radar reflectivity area, echo top heights, and echo-region longevity (Houze and Cheng, 1977). TOGA-COARE results showed the ubiquity of isolated convection as it was present 48 % of the time through the 80 day campaign (Rickenbach and Rutledge, 1997). However, even after these two campaigns, a thorough detailing of many potential length scale characteristics of these ubiquitous clouds is still lacking in the literature. The discussions that do exist tend to be limited by temporal, spatial, or instrument constraints, or study scope (Machado et al., 1993; Mapes and Houze, 1993; Masunaga et al., 2006). This may be partially a function of radar domain sizes. The results of Igel et al. (2014) would seem to suggest why. In that study, it was found that many tropical convective cloud objects are too large to fit in a single ship-borne radar's domain. This idea would certainly be consistent with both the truncation of areal coverage data in

Houze and Cheng (1977) and with the first author's experience operating a radar on board the R/V *Revelle* during the recent Dynamics of the Madden–Julian Oscillation (DYNAMO) campaign (Zhang et al., 2013). Given these limitations, one of the goals of this study is to examine length scales of tropical convection with a new tool well suited to the task for the generation of a global database.

In addition to listing the scales of tropical, deep convection, the results in this paper demonstrate the ways in which convective cores and anvils are related. Results show their mutual growth and interactions. Li and Schumacher (2011) suggested that large-scale areal coverage of anvils and of convecting regions are related in the tropics, with more convective coverage yielding larger anvil coverage. Figure 18c from their manuscript, together with a linear regression through the local maxima of their data suggest a nearly one-to-one relationship of regional anvil coverage to regional convective coverage for convection over tropical oceans. Feng et al. (2012) also note somewhat similar behavior. The applicability of these ideas to individual clouds will be tested. It will be shown here that the relationship between anvils and cores among single-core and multi-core convective storms behave in similar and dissimilar ways and that the differences arise transitionally rather than abruptly as the number of cores increases. It is hoped that by analyzing scales of convection that simple, theoretical insight may be gained regarding the nature of tropical deep convection. Establishing these theoretical ideas is the ultimate goal of this study.

This paper is organized as follows. A brief summary of the methods to be used is given. Then an examination of convective scales is conducted, and relationships between various components of tropical, deep convection are discussed. The analysis of scales begins with an examination of an average cloud, then moves to morphological trends with increasing "pedestal" width and anvil height, and then to a description of cloud structure. Finally some conclusions will be offered on the nature of convective dynamics in the tropics as revealed by examining these scales. Where applicable, these ideas are assessed with a model.

2 Methods

While a thorough description of the methodology is included in Igel et al. (2014) henceforth to be referred to as IDV14, a brief description of the data subset produced by our CloudSat subsampling and cloud object isolation technique is included here. 94 GHz nadir-pointing cloud radar data from CloudSat (Stephens et al., 2008) are used to identify deep convective clouds. Data are taken from the daytime overpass to avoid certain granule issues. Reflectivity, cloud class, and cloud mask thresholds were applied to the data and pixels not meeting these thresholds were shorn away in order to create what have been dubbed, cloud objects. These are regions of contiguous pixels identified as a single cloud object. The regions are then run through a suite of objective analysis tools in order to measure their physical properties and to ensure that they exhibit certain shape characteristics indicative of deep convection. For example, IDV14 are able to separate deep convective "anvils" from their parent "pedestal". The pedestal is the narrower region of the cloud below the anvil. Briefly, this separation was determined by finding local minima in the second vertical derivative of object width. Such a technique is able to determine the level at which convection quickly begins to widen with height. The height at which this occurs in a cloud object is termed the "anvil cutoff height". The methodology requires that an anvil cutoff be found for an object to be included in the database. Further, IDV14 require than the anvil be at least 50 % wider than the pedestal in order to ensure cloud objects are mature. An attempt to count the number of "convective cores" within pedestals is made. In reality, these are just local maxima in reflectivity that may or may not have an active updraft although the results of Li and Schumacher (2011), in which TRMM and CloudSat data are compared, suggest accuracy in the method used here. Reflectivity maxima from ground-based radar are often assumed to mark the position of updrafts (Houze, 1993; Yuter et al., 2005; Luo et al., 2008). Regardless of what physical entities are actually being measured by recording the number of reflectivity maxima, this method should indicate the level of inhomogeneity within the pedestal which is hopefully indicative of the number of cores.

Data are included only if they are tropical (30° S to 30° N) and if the entire object is over ocean. Over 22 000 cloud objects meet the specified requirements and are included in the data analyzed here. Length scales are defined as follows. Cloud top and bottom heights are the heights of the highest and lowest points of the clouds object, respectively. Anvil width is the distance between the two horizontally-farthest apart ends of the cloud object. Pedestal width is calculated as the sum of the width of cloudy pedestal columns and excludes clear columns below anvil base. It's worth noting that the measured anvil cutoff is primarily a measure of the height at which the object transitions in the vertical from pedestal-like, nearly constant width with height, to anvil-like, wide and overhanging clear air or pedestal, characteristics. The cutoff height may not reflect the anvil base height away from the pedestal especially if ice particles fall out from anvil base away from the pedestal. Details are included in IDV14.

When relevant, the results presented in Sect. 3 will be limited to small, isolated convective events by screening the database for cloud objects with few (1 or 2) cores or narrow (< 25 km) pedestal widths. However, other results will necessarily include cloud objects from this scale all the way up to large multi-cellular cloud clusters or mesoscale convective systems since no upper limit on length scales is applied. The goal of the analysis though will be to focus on the most highly populated, smaller scale clouds of the dataset. These objects have often only one or two cores within their pedestals. They have well-developed anvils as a requirement of IDV14, but are unlikely to have organized mesoscale structures. However, as is ultimately demonstrated here, focusing on just the smallest, most frequent deep convective clouds is not necessary as clouds appear to grow smoothly from small to large objects. Several sampling issues are discussed in the appendices.

2.1 The radiative–convective equilibrium simulation

Later in this paper, the results from a large-domain cloud resolving model simulation will be compared to those obtained from CloudSat. The simulation is conducted with the Regional Atmospheric Modeling System (RAMS) (Pielke et al., 1992; Cotton et al.,

2003; Saleeby and van den Heever, 2013) model. The model is integrated forward for a sufficient time such that it achieves a statistical equilibrium (all atmospheric energy and moisture tendencies are negligible) often referred to as a state of radiative-convective equilibrium (RCE) (Manabe and Strickler, 1964). The model is run with a fixed ocean SSTof 300 K and utilizes bulk surface flux parameterizations. A horizontal grid spacing of 1 km is used and 65 vertical levels are employed, which is more than sufficient to meet the moisture resolution requirement of Tompkins and Emanuel (2000). The model is run with a very large number of points in a "canyon" type configuration (Tompkins, 2001) with 3000 "zonal" and 200 "meridional" points. While only 200 km in one direction is rather small to resolve all possible cloud scales, the 3000 km direction allows for more complex, large-scale structures. Periodic lateral boundary conditions are used. RAMS has been used for RCE simulations in the past to understand varous aspects of convective dependencies on, for example, radiation (Stephens et al., 2008), aerosol (van den Heever et al., 2011), and surface temperature (Posselt et al., 2012). This simulation is discussed more fully in Igel et al. (2015), and will be used here simply as a confirmation of an idea that links pedestal and anvil behavior.

3 Results and discussion

3.1 The average cloud

The goal inspiring this study is to quantitatively describe the physical length scales of an average, deep, oceanic convective cloud. Figure 2 shows a composite of all single core cloud objects. IDV14 contains an explanation of how this figure is constructed. Briefly though, Fig. 1 illustrates the percent of cloud objects that would overlap if all cloud object pedestals were centered at the same place in time and space. It might also be thought of as the relative percent of clouds reaching a certain size. The composite point is at the pedestal center below the base. This overlap percentile composite represents the average, approximately symmetric cloud object from the data set at each percentile

threshold. Due to the high variability of cloud object shape, percent values are low. The figure is mostly for visualization of the data and trends therein, and it should not be taken as precisely numerically indicative. The most surprising aspect of this composite is both the width and depth of the anvil. Table 1 includes the statistics of the average cloud as computed using the entire dataset. The mean pedestal width is ∼11 km which is broadly in keeping with mostly graphical (i.e. not specifically enumerated) results from early studies (e.g. Zipser, 1977; Leary and Houze, 1979; Rickenbach and Rutledge, 1997) although this value dwarfs the measured updraft widths of LeMone and Zipser (1980) which tended to be on the order of 1 km. Both the mean and median pedestal widths are approximately 11 km. Mean anvil width is 95 km, which is much larger than many radar studies would be able to measure consistently, given that for a 250 km radius radar domain, a pedestal would need to be centered within 205 km of the radar to contain the entire anvil or within the inner 67 % of the domain. In fact, 95 km very nearly fits the minimum threshold of 100 km to be referred to as a "cloud cluster" in the GATE nomenclature (Houze, 1982), despite this being the average for single core clouds. Interestingly, anvils of ∼100 km (or greater) horizontal scale would be difficult to observe visually as the anvil would stretch beyond the horizon. Also, many ground-based radars may not be especially sensitive to the types of particles making up the anvil.

One of the striking results is the similarity of anvil and pedestal depths (cutoff height in Table 1). There is seemingly no universal conclusion drawn on this subject from the literature (Zipser, 1977, and citations therein). The measured anvil depth (6.4 km) falls within the range of these early observations of anywhere between 1 and 10 km. The inner two-quartile ranges of sizes in Table 1 are often quite large compared to the mean.

An "average cloud" may also be examined for those cloud objects with 2 cores. The mean 2-core pedestal width is almost exactly twice that of the single-core. The anvil width of two-core systems is larger, but not greatly so. As shown in Table 1, cloud top height, anvil cutoff height plus anvil depth, increases with two cores as cloud objects

can presumably grow more easily in the vertical with two cores than with one. The three-or-more core results broadly follow the same trends. Interestingly, the pedestal width of each object divided by its number of cores, a crude measure of the width of convective cores, is ∼12 km per core and remains nearly constant as the number of cores increases.

The composite image of cloud objects with 2 or more cores (Fig. 1) is much wider and appears to exhibit structural characteristics consistent with MCSs (Houze, 2004). It has a wide pedestal and deep anvil across a wide range of percentiles unlike the single cell composite. The highest overlap percent is centered in the mid-troposphere, whereas in the single core composite it is centered in the lower troposphere. This result shows the comparative similarity of mid-level structures in multi-celled clouds compared to single cells and may imply differences in the updraft structure as described by Luo et al. (2008). The statistics bear out a colder cloud top and wider anvil. The causes and implications of some of these results will be revisited later.

Interestingly, pedestal top or anvil base (cutoff) height stays almost constant from one to two to potentially many core systems, although there is a statistically significant difference in the population of lower cutoff heights in the three-or-more core clouds than either the single or double core clouds as determined by a two-sided t-test at a 95 % confidence level. However, it is primarily the anvil depth that changes in such a way as to increase the total cloud object height as core number increases. These trends hint at different roles for cloud objects with different core numbers. Single-core clouds have an anvil area that is already ∼30 % as wide as the 3-or-more-core cloud objects. Assuming constant mass flux per core, the small increase in anvil width with increasing core number would imply much more detrainment into the environment per amount of convective mass flux for single core cloud objects than for multi-core cloud objects. Perhaps this helps to explain why single-cell clouds often precede multi-cell clouds (e.g. Leary and Houze, 1979). Single-cell clouds might moisten the environment because they flux proportionally too much mass out of their anvils (i.e. perhaps they have low precipitation efficiency [the ratio of liquid/ice precipitated to that of vapor

fluxed through the cloud base (Cotton et al., 1995)]); then, multi-cell clouds could form in the newly moistened environment from where they may rain out the excess vapor (i.e. perhaps they have high precipitation efficiency). The dynamics of this evolution are unclear from this study, but the concept is logically consistent from a system perspective. These ideas have been suggested previously and are conceptually coherent with studies showing the importance of MCSs to total rain production (e.g. Mohr et al., 1999; Nesbitt et al., 2006; Rossow et al., 2013; Barnes and Houze, 2013).

3.2 Pedestal widths

In this section, details of trends in convective quantities with increasing pedestal widths will be discussed. In order to help build the conceptual model of clouds that will be the result of this study, pedestal width necessarily will be treated here independently from all other meteorological and morphological quantities with the assumption that the local convection itself dictates its own pedestal width.

The basic trends in morphology with increasing pedestal width are shown in Table 2. Unsurprisingly, the number of counted cores increases with pedestal width. In fact, many of the trends are conceptually consistent with increasing cores (as in the previous section). That the anvil cutoff height characteristics are so similar between clouds with pedestal widths less than 25 km and clouds with pedestal widths between 25 and 50 km is noteworthy despite the other differences between these groups of clouds.

Anvil width tends to increase with pedestal width. To our knowledge, the way in which anvil and pedestald widths should be related has not been proposed in the literature from either observations or theory. From Table 2, the mean pedestal width for clouds at narrow pedestal widths (< 25 km) is ~ 13 % as wide as the corresponding anvil while that of the wide pedestal width (> 50 km) is ~ 38 %. This result fits well with the latter results presented in Sect. 3.1. Although it should be noted that the minimum anvil width is required to increase with pedestal width since the anvil must be wider than the pedestal.

Individual cloud object pairs of pedestal and anvil widths are plotted in Fig. 2a. Due to the inclusion of a minimum detrainment index (Bacmeister and Stephens, 2011; IDV14), cloud objects are required to have an anvil width to pedestal width ratio of at least 1.5. There is considerable spread in the data shown in Fig. 2a given the large number of cloud objects and many different evolutions of different clouds. Figure 2a is constructed to emphasize this spread; Fig. 3b (discussed next) is constructed to emphasize the trend of the data. Despite the large vertical spread in the data, many of the data points lie just above the cutoff of an anvil to pedestal width ratio of 1.5. Consequently, a simple linear regression fit has a slope of 1.9 as shown in the dashed gray line. The scatter of ratios of anvil width to pedestal width is shown in Fig. 2b. The figure shows that the mean ratio decrease as pedestal width increases. Table 2 implies the same result – the ratio of anvil width to pedestal width for cloud objects with pedestal widths of less than 25 km is 7.4 while for the ratio of those larger than 50 km is only 2.7. The change in ratio of anvil width to pedestal width suggests that as pedestals grow, anvil overlaying clear air becomes a smaller portion of the total cloud width.

Figure 3a shows a slightly different kind of regression fit for the data. The data are binned logarithmically by pedestal width. The bins are logarithmically spaced to account for the relative paucity of data at high pedestal widths. The mean of anvil widths within each bin is calculated. Then, powers of pedestal width are taken in an attempt to linearize the data in order to better fit a simple linear regression. Pedestal width to the 2/3rd power was determined to yield the best correlation coefficient (for the linearized data) for the available data and yielded the lowest mean square error (MSE). The MSE and R squared values for pedestal width to the 2/3 power were better than those of linear, logarithmic, or exponential fits by between 3 and 90 %. The residuals of the regression were much better behaved for the 2/3 fit than for the linear or exponential fits especially at low and high pedestal widths. These regressions were also calculated for random subsamples of half the population of data multiple times to the same conclusions. Figure 3b shows counts of data in pedestal width-anvil width bins. The 2/3 power-law regression fit can be seen to approximate well the local population

and general trend of the cloud objects. This implies that statistically, as a fraction of the original width, anvil widths grows at a retarded rate relative to pedestal width. This result is consistent with the results in the previous section. The anvil width is found to depend on pedestal width in the following way

$$W_A = 14\ \text{km}^{1/3} \cdot W_P^{2/3} + 19\ \text{km}, \quad (1)$$

where W's are widths in meters, and subscripts A and P indicate anvil and pedestal values, respectively. The ratio of W_A to W_P then becomes

$$\frac{W_A}{W_P} = \frac{14\ \text{km}^{1/3}}{W_P^{1/3}} + \frac{19\ \text{km}}{W_P} \quad (2)$$

which is monotonically decreasing as a function of pedestal width. Furthermore, it is evident that Eq. (2) predicts very well the mean pedestal width-anvil width pairs in Tables 1–3. The non-zero intercept in Eq. (1) and in the regression fit in Fig. 2a indicate a small amount of uncertainy in the selection of cloud objects and the limitations of using data with discrete along-track resolution.

Let us introduce a useful thought experiment in order to explain this 2/3rd power, empirical relationship. This derivation is not meant to be strictly applicable to any one cloud but to the ensemble growth of many clouds similar to the ensemble from which the 2/3 scaling was suggested. If a deep convective cloud can be thought of as a pedestal that fluxes mass into an anvil, then a simple geometric construct can be imagined that helps to explain this 2/3 parameter value. Assuming morphological isotropicity in the mean, then a convective pedestal is approximately cylindrical with its axis oriented vertically. Neglecting any lateral organized detrainment or stochastic entrainment through the sides of the cylinder, the cloud fluxes mass up through the depth and out through the top of the cylinder. Thus, the total flux through the pedestal is

$$F_P = \rho \pi R_P^2 w, \quad (3)$$

where F_P is the mass fluxing out of the pedestal top, ρ is the air density, R_P is the pedestal radius, and w is the flux velocity. Anvils might be thought of as a spherical balloon being filled by the mass fluxing out of the top of the core within the pedestal. When integrated from the initial time of anvil genesis to some final time, its mass flux is

$$F_A = \rho \frac{4}{3} \pi R_A^3 \Big/ \Delta t, \quad (4)$$

where F_A is the anvil flux (total mass per total time) and R_A is the anvil radius. Upon equating the fluxes and performing some algebra, the expectant relationship between anvils and pedestals is

$$R_A = \sqrt[3]{\frac{3}{4} w \Delta t R_P^2} = \sqrt[3]{\frac{3}{4} w \Delta t} R_P^{2/3} = \alpha R_P^{2/3} \quad (5)$$

where α is just the third root of the proportionality constants. For simplicity, the densities are assumed to be the same and hence to cancel in Eq. (5), but if they don't, R_A's functional dependence on R_P is unchanged with α absorbing some factors of relevant densities.

In the mean (see Table 1), anvils are much wider than they are deep and are non-spherical. In such a case, an anvil may be assumed to be ellipsoidal with major axes in the horizontal plane and the corresponding flux relationship is

$$F_A = \rho \frac{4}{3} \pi R_1 R_2 D / \Delta t \quad (6)$$

with R_1, R_2, and D representing the different major axes, radius 1, radius 2, and depth, respectively, of the ellipsoid. As long as each length continues to grow as any other one of them does, such that, for example, R_2 and D are both linear functions of R_1, then $R_1 \cdot R_2\,(R_1) \cdot D(R_1)$ results in a third power of R_1 and a functional 2/3 power may reasonably hold. Assuming isotropicity, R_2 is equal to R_1. In the data, it turns out that D is only a very weak function of R_1 where R_1 is taken to be one half the measured anvil

width and D is the anvil depth (not shown but implied by Table 2). Of course, these derivations are far from physically precise predictors of anvil growth for any one cloud. The goal is only to derive the basic functional form suggested by the 2/3 scaling for the entire population of clouds or at the very least to suggest why the mean anvil-to-pedestal width ratio decreases as pedestals widen.

A 2/3 scaling relationship seems to fit across a wide range of horizontal scales – from single to many cored systems. Figure 4 shows the scaling relationship for just single and double core cloud objects and for clouds objects with 4 or 5 cores in order to assess its relevance across differing cloud systems. It is apparent from the figure that a 2/3 scaling results in an approximately linear fit for both of these datasets. It would seem that the physics governing the interrelationship between pedestals and anvils is somehow similar among differently organized clouds. The most significant difference between the two lines in Fig. 4 is the range over which the bins occur. In the region of pedestal width overlap, 11–70 km or $(500\,\mathrm{m})^{3/2}$–$(1700\,\mathrm{m})^{3/2}$, the means of the data are very similar. The single and double core data exhibit weak gradients in the mean below 11 km or $(500\,\mathrm{m})^{3/2}$. This result is likely the consequence of narrow, young anvils strongly growing before the cloud can develop an organized flow structure and potentially from some contamination of the data by small pedestals convecting into existing anvil cloud although these occur infrequently (IDV14).

These results may provide a possible explanation for the poor correlation between convective core (pedestal) coverage and anvil coverage presented in Li and Schumacher (2011) and Feng et al. (2012). These studies did not take into account the power-law non-linearity observed here (or any), although what is being measured in these previous papers is slightly different from what is being described here, even if the aims are similar. While these other studies tended to focus on slightly larger objects than are the focus of this study, our results are inclusive of their scales.

Finally, the Appendices below contain a variety of geometric arguments concerning sampling of clouds. These are especially relevant to the 2/3 scaling. Briefly, it is determined that off center sampling of cloud objects is unlikely to influence the form of the

scaling but could influence the precise regression coefficients. It is also found that even if cloudy regions are not horizontally circular, the numbers quoted herein are unlikely to be far from the true characteristic horizontal length scales of convection.

3.3 Anvil top height

Tropical, deep convective clouds of all types contribute to both local and global scale circulations. Riehl and Malkus (1958) estimated the contribution of undiluted hot towers to the Hadley circulation. Gray (1973) and Houze (1982) considered the effects of convection on regional circulations at the convective- and meso- scales. There is currently no way to examine explicitly such responses to convection from any current satellite since no earth observation platform provides any direct measure of air velocities above the surface level either in cloud or clear air. An attempt will be made to infer such contributions per cloud object by using the clouds as a simple diagnostic.

In convective circulations, air is forced upward through convective cores and then outward through anvils (e.g. Riehl and Malkus, 1958; Emanuel et al., 1994). Deep convection actually pushes upper tropospheric air through dynamic pressure perturbation (see next section). At first glance, it might be assumed that horizontally wider anvils are more likely to contribute circulations farther from the updraft core than narrower ones. That is to say, that it could be assumed that wide anvils are the result of and a tracer of a cloud's ability to influence the motion of air over a large area and therefore could be an indication of the cloud's contributing to large-scale, horizontal circulations. If this assumption, that in the ensemble mean, wider clouds are better able to influence upper level horizontal flow than narrower clouds, can be made, then other cloud morphological quantities can be regressed against anvil width to determine their role on large-scale circulations. Figure 5a shows the scatter of anvil widths and anvil top height with the best-fit linear regression line. Figure 5b shows counts of cloud objects in cloud top height-anvil width bins. From the regressions in this figure, it would seem that higher topped anvils are horizontally wider on average although the trend is weak. The average cloud top height for a cloud with an anvil width of less than 100 km is 13.6 km;

whereas for those wider clouds, the average top height is 14.8 km. So, it would seem that wider, more organized cloud systems are better able to produce strong updrafts and reach higher altitudes than narrower cloud systems. A similar result could be deduced from Cetrone and Houze (2006) who implicated subtle humidity increases as resulting in larger overall clouds. Yuan and Houze (2013) also made analogous conclusions (wider and higher clouds). To first order, it would seem possible from Fig. 5 that higher topped clouds can contribute more mass to large-scale circulations. Differences in theoretical heating profiles between young and mature convection in which mature convective heating exhibits a greater magnitude at high altitudes (e.g. Schumacher et al., 2004) and between observed heating profiles of wide and narrow precipitation features (Liu et al., 2015) imply a similar result.

3.4 Comparisons to the simulation

It is worth testing some of these observationally derived conclusions against results from the RCE simulation described above. In principle, none of the above results are in any way built into RAMS. However, if the RCE simulation exhibits some of the same pedestal-anvil behavior, then a compelling case can be made that these results are in some way fundamental to the physics of clouds at scales resolvable even at 1km horizontal grid spacing.

3.4.1 2/3 scaling

To examine whether the RCE simulation exhibits a 2/3 scaling, a simple RCE object identification and anvil cutoff algorithm were implemented for the model output. Cloud objects were defined to be contiguous cloudy grid boxes of total condensate mixing ratios of greater than 0.01 g kg^{-1} that stretched from 1 km above the surface to 11 km in order to be consistent with the CloudSat data. They are sampled along the long axis of the simulation to yield 2-dimensional width-height cross-sections reminiscent of the CloudSat objects. An anvil cutoff height was determined for each RCE cloud object by

subjecting each object to the cutoff algorithm (IDV14) used on the CloudSat objects with only minor changes made to accommodate the different data. Results are shown in Fig. 6. It can be seen that while a 2/3 scaling does exist in the simulation data, it is less well constrained due, at least in part, to significantly fewer data samples from the simulation than the observations. The range of cloud sizes for which this analysis is valid is much less than that observed by CloudSat due in part to limitations imposed by the domain size. However, it is encouraging that such a relationship is evident in the CRM simulation at all, and its suggestion helps to corroborate the observational result. Because the model is run with a fixed SST of 300 K, the relationship shown in Fig. 3a was recreated by limiting the CloudSat data to clouds with SSTs between 299.5 and 300.5 K (not shown). The 2/3 fit remained appropriate.

3.4.2 Anvil dynamics

One of the primary goals of this study is to assess the physical links between convective pedestals and anvils. To help to form a direct kinematic link between pedestals and anvils, a composite cloud has been made from the simulated output. Figure 7a shows the composite cloud vertical velocity field in colored contours and the median cloud outline in thick white. The horizontal dashed line indicates the mean level of the objectively found anvil-cutoff height. The most striking result of this composite is the colocation between the maximum velocity and the anvil-cutoff height. Figure 7b show the horizontal divergence implied by the vertical velocity composite in Fig. 7a. Through this application of anelastic continuity (for simplicity) it can be seen that horizontal divergence occurs at all levels in the convective column above the vertical velocity maximum. Consequently the base of the anvil occurs at the level of the velocity maximum as air is dynamically forced outward above. Figure 7b shows that maximum divergence occurs just below the tropopause layer (14–18 km) (Fueglistaler et al., 2009). The maximum in divergence might be a result of capping by the tropopause or neutral buoyancy processes. Certainly this idea cannot be rebutted conclusively here. However, it could be suggested that the vertical asymmetry in horizontal divergence is unlikely to result from

cloud vertical velocity maxima colliding with a level of neutral buoyancy. In the tropics where temperature profiles are rarely very far from moist-convectively neutral stability, the level of neutral buoyancy is unlikely to be strictly deterministic. In fact, the results of Takahashi and Luo (2012) suggest only a weak control by the level of neutral buoyancy on tropical deep convection.

Additionally, it could also be asked why the velocity maximum and anvil base, occur at the height that they do. We suggest it is the result of microphysics within the pedestal. Previous investigations have shown that the mid-tropospheric velocity maximum in deep convection is the result of latent heating of deposition (Fierro et al., 2012; Storer and van den Heever, 2013; McGee and van den Heever, 2014). This depositional heating positively accelerates convecting air parcels. Figure 7c confirms this assumption. The figure shows a composite of depositional heating rates from the RCE simulation. It is important to remember that depositional heating results in an acceleration of the velocity field and so should be maximally important below the level of peak velocity. Because of the accumulated acceleration due to deposition, the vertical velocity peaks at ∼ 8 km. Above the velocity peak, air begins to diverge thereby forming an anvil.

3.4.3 Fixed lower-anvil temperature

In IDV14, it was shown that anvil base temperature remains fixed across different SSTs. This response was dubbed the Fixed Lower-Anvil Temperature (FLAT) hypothesis. Previously, it was suggested that some balance might exist at the lower edge of the anvil between a variety of temperature-dependent diabatic processes that would keep mean anvil base temperature constant across a wide range of deep convective clouds. The RCE simulations seem to indicate that the arguments in IDV14 are potentially only partially correct. The parameterized processes that control microphysical deposition onto ice species are strong functions of temperature in RAMS (Walko et al., 2000) and reality (Wexler, 1977). Since deposition controls the anvil base height, and since temperature controls deposition, it should be that temperature controls anvil base height.

This temperature control would not depend on surface or climate conditions. The validity of FLAT could be further tested in the future by altering the temperature dependence of deposition in RCE and other numerical simulations.

The mean height of the velocity maximum seen in these clouds is somewhat lower than in recent observations by Heymsfield et al. (2010). The maximum is ∼ 9 km in the simulated clouds while at ∼ 10.5 km in the subset of oceanic clouds in their Fig. 7c. Although, the results here are not dissimilar quantitatively or conceptually to those presented in Mapes and Houze (1995) and Yuter and Houze (1995). However, much of their convection seems to reach generally higher heights than the clouds in this simulation which often top out around 14 km. Furthermore, the differences observed are only indicative of height, not temperature – which is the more important quantity to the arguments being made for FLAT. Finally, it is noted that FLAT implies that the total depth of anvils may not only be the consequence of mass building down from the anvil top's being capped by the tropopause or level of neutral buoyancy but also from a bottom up process resulting from the convergence of mass at the midlevel velocity maximum.

4 Conclusions

The discussion above has focused on analyzing cloud scales from a unique CloudSat dataset of mature deep convective clouds (IDV14). It was one of the goals of this paper to list and discuss length scales of these clouds. The "average cloud" was discussed for single, double and many core clouds. Cloud sizes tended to be large, on the order of tens to hundreds of kilometers, for the oceanic convection investigated here.

Another central goal of this paper was to better understand the interrelationships between and among various components of deep, convective clouds through the enumeration of length scales. Of primary consequence was the scaling relationship exhibited between anvil and pedestal widths that was shown to follow potentially a 2/3 power. Thus, anvils become progressively more underlain by pedestals as cloud width grows.

This particular power led to the suggestion that deep convective clouds flux convective mass through a cylindrical convective pedestal into a spherical (more likely, ellipsoidal) anvil such that the 2/3 power is a fundamental result of 3 dimensional space. The question then becomes to what extent this 2/3 scaling is predictive in the mean. If it has any power to predict anvil width based on pedestal width, then a physically based anvil width parameterization scheme might be created. Of course, such a scheme could only maximally be as accurate as the prediction of pedestal width. This avenue could be something for modelers to consider. Anvil top height was subsequently examined in an attempt to determine which kinds of tropical clouds (single-core or MCSs) are taller. It was found that wider, more orgnized cloud objects generally obtain higher cloud top heights than narrower ones. Finally, some of these CloudSat results were compared with results from a large domain RCE simulation. While the statistical fit was not as good as for the observations, a 2/3 scaling was still apparent in the simulation data. The temperature dependence of depositional growth of ice species was implicated as a potential explanation for the FLAT response seen in IDV14.

In concluson, these results demonstrate that as cloud pedestal width grows, a number of morphological and physical changes appear to occur in cloud objects. The anvil widens but at a slower rate than the pedestal. The number of cores increases, the cloud base height drops, and the cloud top rises. This theory, the stretched building block hypothesis (Mapes et al., 2006), is, in contemporary understanding, well established locally. However, this study, which utilizes 5 years of tropics-wide observational data, serves to illustrate the theory's applicability to the global tropics. Finally, it was suggested that as pedestal width grows, individual cloud objects become increasingly influential to circulations and precipitation – a result that also complements contemporary theory.

Appendix A: Off-center sampling

It has been implicitly assumed throughout the analysis that CloudSat's curtain-type sampling of clouds does not introduce any biases in the data. In this appendix, we will show that the effects of sampling along track do not affect greatly the kinds of relationships derived above.

It has been assumed throughout this manuscript that clouds objects are quasi-circular in the horizontal and it will be assumed here. Figure A1 shows a potential anvil/pedestal combination in plan view. The outer circle is meant to trace the edge of the anvil; the inner circle traces the pedestal edge. The radii of the pedestal and anvil are labeled as R_p and R_a, respectively. Thus, the true anvil radius to pedestal radius ratio is R_a / R_p for the object in the figure. The gray lines labeled A–D represent possible CloudSat orbits that would sample this cloud object. Transect A would not yield a cloud object as it does not sample the pedestal. However B through D would result in cloud objects. Each sample of this single cloud would yield a different pedestal to anvil width ratio. But how important is this?

Determining this is mathematically tractable. If the sampled radius of the cloud is defined to be along the x axis, with the sampled pedestal distance defined as x_p and the sampled anvil distance defined as x_p, then the equation of the circles defined by R_a and R_p at any y value are:

$R_p^2 = x_p^2 + y^2$ and
$R_a^2 = x_p^2 + y^2$.

Upon trivially rearranging and taking the ratio of x_p to x_p:

$$\frac{x_p}{x_p} = \sqrt{\frac{R_a^2 - y^2}{R_p^2 - y^2}}.$$

Figure A2 shows the result of this equation for values of R_a and R_p of 100 and 50 km, respectively. This results in an assumed ratio of R_a to R_p of 2-to-1. Values in Fig. A2 are normalized by this ratio (i.e. $[x_p/x_p]/2$). Curly braces will be used below to indicate a value is normalized by the true ratio, R_a / R_p. The value of 2 in the figure exaggerated the importance of sampling issues as the lower this ratio is, the higher the mean x_p to x_p since the ratio depends on the difference between R_a and R_p. It can be seen from Fig. A2 that while the true R_a / R_p is 2 that the measured x_p/x_p is everywhere higher than 2 $\{1\}$. However, for the lowest 90 percent of ratios the mean x_p/x_p is 2.4 $\{1.20\}$. While for the lowest 50 percent of ratios, the mean x_p/x_p is only 2.1 $\{1.04\}$. This is a mean high bias of only 10 % for the lowest 50 % of samples. But, a R_a / R_p of 2 is actually rather low. For a more physically relevant R_a / R_p of 10 like that of the "average cloud" from above, the mean x_p/x_p below the 90th percentile is 12.8 $\{1.28\}$, and the 50th percentile mean x_p/x_p is only 10.7 $\{1.07\}$.

Given these values, it is possible to artificially resample our data. By creating PDFs of all relevant real R_a / R_p and randomly sampling from among and within these distributions to adjust our cloud objects, we get these new PDFs of pedestal widths and anvil widths. Each data point is randomly sampled from within the PDF at values of x_p less than R_p. This process is run many times and new, synthetic data sets are created. The new, raw datasets look similar to the original dataset except for an approximately linear shift toward higher synthetic x_p and lower x_p/x_p.

For a wide variety of true R_a / R_p values, it can be shown that only the top 10 % of x_p/x_p values are likely to be greatly affected by sampling biases. If these top 10 % are synthetically eliminated from the dataset, a new scatter can be created. While the precise regression fit changes to reflect the lack of high x_p/x_p's (higher slope, lower intercept), the linearity of a $x_p/x_p^{2/3}$ fit is little diminished. The biggest concern is that these measurement biases somehow yield an artificial 2/3 scaling in our data, but this does not appear to be the case analytically or numerically.

It will also be mentioned here that fractal theory would suggest that any cloud edge is not perfectly circular (Lovejoy, 1982). Cloud area is a function of diameter as

$$A = \sqrt[1.35]{(\pi D)^2}$$

with the obvious functional deviation from the equation for a circle being the 1.35 power root. The addition of this root would complicate our results. It would imply that the assumption of circularity becomes less good for larger cloud component widths. There may be some evidence of this when the data is rank ordered. When extended out to very large diameters (700 km), the linearity of the scattered data decreases.

Appendix B: Non-circular objects

There also arises the issue of non-circular but still geometric anvils in the horizontal plane. Cetrone and Houze (2006) state that their echo objects were often oriented at ±45° to the pole once only objects with an ellipsoidal axis ratio of 1.5 or greater had been accounted for. The mean axis ratio of their ellipsoidal echo objects was 2.4. Liu and Zipser (2013) find that ∼ 70 % of their precipitation features (approximately a "cloud object" here) have axis ratios between 1.5 and 10. The radius measured of an ellipse at 45° to its major axis is

$$R_m = \sqrt{2^{a^2 b^2}/a^2 + b^2}$$

Upon applying the results of Cetrone and Houze (2006), R_m becomes 1.31. The area of the actual echo object would be $\pi \cdot 2.4$ whereas the implied circular area would be $\pi \cdot 1.31^2$ or $\pi \cdot 1.70$. This means the circularity assumption could be off by as much as −40 % on average. However, if we assume the variance is such that the orientation varies from 30 to 60 with regularity, then the assumption will be off by −53 to +10 %

with radii factors or 1.26 to 2.63. Thus assuming anvils are circular is likely to underrepresent their area by ∼21 %. However, their measured radii should be decently representative of the characteristics radius of any individual object. And again, it should be reiterated that these calculations are for objects that are preselected to be ellipsoidal and for mean not median values of axis ratios. So while admitting the potential bias in scales observable from the dataset developed in IDV14, it will be stated that only worst case scenarios are likely to be of concern.

Acknowledgements. This work was supported by NASA through CloudSat grant 5-319160 and by NASA Headquarters under the NASA Earth and Space Science Fellowship Program – Grant NNX 13AN66H. The authors would like to acknowledge the contributions of A. Drager. The authors would also like to thank E. Riley and E. Barnes for their helpful suggestions.

References

Bacmeister, J. T. and Stephens, G. L: Spatial statistics of likely convective clouds in CloudSat data, J. Geophys. Res, 116, D04104, doi:10.1029/2010JD014444, 2011.

Barnes, H. and Houze, R.: The precipitating cloud population of the Madden-Julian Oscillation over the Indian and west Pacific Oceans, J. Geophys. Res, 118, 6996–7023, 2013.

Cetrone, J. and Houze, R. A.: Characteristics of Tropical Convection over Ocean near Kwajalein, Mon. Weather Rev., 134, 834–853, 2006.

Che, S. S., Houze, R. A., and Mapes, B. E.: Multiscale Variability of Deep Convection in Relation to Large-Scale Circulation in TOGA COARE, J. Atmos. Sci, 53, 1380–1409, 1996.

Cotton, W. R., Alexander, G. D., Hertebstein, R., Walko, R. L., McAnelly, R. L., and Nicholls, M.: Cloud Venting – a review and some new global annual estimates, Earth.-Sci. Rev., 39, 169–206, 1995.

Cotton, W. R., Pielke Sr., R. A., Walko, R. L., Liston, G. E., Tremback, C. J., Jiang, H., McAnelly, R.L., Harrington, J. Y., Nicholls, M. E., Carrio, G. G., and McFadden, J. P.: RAMS 2001: Current status and future directions, Meteor. Atmos. Phys., 82, 5–29, 2003.

Emanuel, K. A., Neelin, J. D., and Bretherton, C. S.: On large-scale circulations in convecting atmospheres, Q. J. Roy. Meteorol. Soc., 120, 1111–1143, 1994.

Feng, Z., Dong, X., Xi, B., McFarlane, S. A., Kennedy, A., Lin, B., and Minnis, P.: Life cycle of midlatitude deep convective systems in a Lagrangian framework, J. Geophys. Res, 117, D23201, doi:10.1029/2012JD018362, 2012.

Fierro, A. O., Zipser, E. J., LeMone, M. A., Straka, J. M., and Simpson, J.: Tropical Oceanic Hot Towers: Need They Be Undilute to Transport Energy from the Boundary Layer to the Upper Troposphere Effectively? An Answer Based on Trajectory Analysis of a Simulation of a TOGA COARE Convective System, J. Atmos. Sci., 69, 195–213, 2012.

Fueglistaler, S., Dessler, A. E., Dunkerton, T. J., Folkins, I., Fu, Q., and Mote, P. W.: Tropical tropopause layer, Rev. Geophys. 47, RG1004, doi:10.1029/2008RG000267, 2009.

Gray, W. M.: Cumulus Convection and Larger Scale Circulations 1. Broadscale and Mesoscale Considerations, Mon. Weather Rev, 101, 839–855, 1973.

Heymsfield, G. M., Tian, L., Heymsfield, A. J., Li, L., and Guimond, S.: Characteristics of Deep Tropical and Subtropical Convection from Nadir-Viewing High-Altitude Airborne Doppler Radar, J. Atmos. Sci., 67, RG4003, doi:10.1175/2009JAS3132.1, 2010.

Holle, R.: Some Aspects of Tropical Oceanic Cloud Populations, J. App. Meteor., 7, 173–183, 1968.

Houze, R. A.: Cloud clusters and large-scale vertical motions in the Tropics, J. Meteor. Soc. Japan., 60, 396–410, 1982.

Houze Jr., R. A.: Cloud Dynamics, Academic Press, 573 pp., 1993.

Houze Jr., R. A.: Mesoscale Convective Systems, Rev. Geophys., 42, RG4003, doi:10.1029/2004RG000150, 2004.

Houze, R. A. and Betts, A. K.: Convection in GATE, Rev. Geophys. Space Phys., 19, 541–576, 1981.

Houze, R. A. and Cheng, C.: Radar characteristics of tropical convection observed during GATE: Mean properties and trends over the summer season, Mon. Weather Rev., 105, 964–980, 1977.

Igel, A. L., Igel, M. R., and van den Heever, S. C.: Make It a Double? Sobering Results from Simulations Using Single-Moment Microphysics Schemes, J. Atmos. Sci., 72, 910–925, doi:10.1175/JAS-D-14-0107.1, 2015.

Igel, M. R.: A Tropical Radiation and Cloud System Feedback Modulated by Sea Surface Temperatures, M.S. thesis, Dept. Atmos. Sci., Colorado State Univ., Fort Collins, Colorado, USA, 2011.

Igel, M. R., Drager, A. J., and van den Heever, S. C.: A CloudSat Cloud-Object Partitioning Technique and Assessment and Integration of Deep Convective Anvil-Climate Feedbacks, J. Geophys. Res. Atmos, 119, 10515–10535, doi:10.1002/2014JD021717, 2014.

Johnson, R. H., Rickenbach, T. M., Rutledge, S. A., Ciesiekski, P. E., and Schubert W. H.: Trimodal characteristics of tropical convection, J. Climate, 12, 2397–2418, 1999.

Leary, C. A. and Houze, R. A.: The Structure and Evolution of Convection in a Tropical Cloud Cluster, J. Atmos. Sci., 36, 437–457, 1979.

Li, W. and Schumacher, C.: Thick Anvils as Viewed by the TRMM Precipitation Radar, J. Climate, 24, 1718–1735, 2011.

Liu, C. and Zipser, E.: Regional variation of morphology of organized convection in the tropics and subtropics, J. Geophys. Res., 118, 453–466, doi:10.1029/2012JD018409, 2013.

Liu, C., Shige, S., Takayabu, Y. N., and Zipser, E.: Latent Heating Contribution from Precipitating Systems with Different Sizes, Depths, and Intensities in the Tropics, J. Climate, 28, 186–203, doi:10.1175/JCLI-D-14-00370.1, 2015.

Lopez, R. E.: Radar Characteristics of the Cloud Population of Tropical Disturbances in the Northwest Atlantic, Mon. Weather Rev., 104, 268–283, 1976.

Luo, Z., Liu, G. Y., and Stephens, G. L.: CloudSat adding new insight into tropical penetrating convection, Geophys. Res. Lett., 35, L19819, doi:10.1029/2008GL035330, 2008.

Machado, L. A. T. and Rossow, W. B.: Structural Characteristics and Radiative Properties of Tropical Cloud Clusters, Mon. Weather Rev., 121, 3234–3260, 1993.

Malkus, J. S. and Riehl, H.: Cloud Structure and Distributions Over the Tropical Pacific Ocean, Tellus, 16, 275–287, 1964.

Manabe, S. and Strickler, R. F.: Thermal equilibrium of the atmosphere with a convective adjustment, J. Atmos. Sci., 21, 361–385, 1964.

Mapes, B. E.: Equilibrium vs. Activation Control of Large-Scale Variations of Tropical Deep Convection, in the Physics and Parameterization of Moist Atmospheric Convection, 321–358, Kluwer Academic Publishers, Boston, MA, 1997.

Mapes, B. E. and Houze, R. A.: Cloud Clusters and Superclusters over the Oceanic Warm Pool, Mon. Weather Rev., 121, 1398–1415, 1993.

Mapes, B. E. and Houze, R. A.: Diabatic Divergence Profiles in Western Pacific Mesoscale Convective Systems., J. Atmos. Sci., 52, 1807–1828, 1995.

Mapes, B., Tulich, S., Lin, J., and Zuidema, P.: The mesoscale convection life cycle: Building block or prototype for large-scale tropical waves?, Dyn. Atmos. Oceans., 42, 3–29, doi:10.1016/j.dynatmoce.2006.03.003, 2006.

Masunaga, H., L'Ecuyer, T. S., and Kummerow, C. D.: Variability in the Characteristics of Precipitation Systems in the Tropical Pacific. Part I: Spatial Structure, J. Climate, 18, 823–840, 2006.

McGee, C. J. and van den Heever, S. C.: Latent Heating and Mixing Due to Entrainment in Tropical Deep Convection, J. Atmos. Sci., 71, 816–832, doi:10.1175/JAS-D-13-0140.1, 2014.

Mohr, K. I. and Zipser, E. J.: Mesoscale Convective Systems Defined by Their 85-GHz Ice Scattering Signature: Size and Intensity Comparison over Tropical Oceans and Continents, Mon. Weather Rev., 124, 2417–2437, 1996.

Mohr, K. I., Famiglietti, J. S., and Zipser, E. J.: The Contribution to Tropical Rainfall with respect to Convective System Type, Size, And Intensity Estimated from the 85-GHz Ice-Scattering Signature, J. Appl. Meteor., 38, 596–606, 1996.

National Academy of Sciences: Plan for US Participation in GARP Atlantic Tropical Experiment. Report of the Ad Hoc Tropical Task Group to the US Committee for the Global Atmospheric Research Program, National Research Council, Washington DC, 25 pp., 1971.

Nesbitt, S. W., Cifelli, R., and Rutledge, S. A.: Storm Morphology and Rainfall Characteristics of TRMM Precipitation Features, Mon. Weather Rev., 134, 2702–2721, 2006.

Pielke, R. A., Cotton, W. R., Tremback, C. J., Lyons, W. A., Grasso, L. D., Nicholls, M. E., Moran, M. D, Wesley, D. A., Lee, T. J., and Copeland, J. H.: A comprehensive meteorological modeling system RAMS, Meteor. Atmos. Phys., 49, 69–91, 1992.

Posselt, D. J., van den Heever, S. C., Stephens, G. L., and Igel, M. R.: Changes in the interaction between tropical convection, radiation and the large scale circulation in a warming environment, J. Climate, 25, 557–571, 2012.

Rickenbach, T. M. and Rutledge, S. A.: Convection in TOGA COARE: Horizontal Scale, Morphology, and Rainfall Production, J. Atmos. Sci., 55, 2715–2729, 1997.

Riehl, H. and Malkus, J. S.: On the Heat Balance in the Equatorial Trough Zone, Geophsyica, 6, 503–538, 1958.

Riley, E. M., Mapes, B. E., and Tulich, S. N.: Clouds Associated with the Madden-Julian Oscillation: A New Perspective from CloudSat, J. Atmos. Sci., 68, 3032–3051, doi:10.1175/JAS-D-11-030.1, 2011.

Rossow, W. B., Mekonnen, A., Peal, C., and Goncalves, W.: Tropical Precipitation Extremes, J. Climate, 26, 1457–1466, 2013.
Saleeby, S. M. and van den Heever, S.C.: Developments in the CSU-RAMS Aerosol Model: Emissions, Nucleation, Regeneration, Deposition, and Radiation, J. Appl. Meteor. Climatol., 52, 2601–2622, doi:10.1175/JAMC-D-12-0312.1, 2013.
Schumacher, C., Houze Jr., R. A., and Kraucunas, I.: The Tropical Dynamical Response to Latent Heating Estimates Derived from the TRMM Precipitation Radar, J. Atmos. Sci., 61, 1341–1358, 2004.
Stephens, G. L., Vane, D. G., Tanelli, S., Im, E., Durden, S., Rokey, M., Reinke, D., Partain, P., Mace, G. G., Austin, R., L'Ecuyer, T., Haynes, J., Lebsock, M., Suzuki, K., Waliser. D., Wu, D., Kay, J., Gettelman, A., Wang, Z., and Marchand, R.: CloudSat mission: Performance and early science after the first year of operation, J. Geophys. Res., 113, D00A18, doi:10.1029/2008JD009982, 2008.
Stephens, G. L., van den Heever, S. C., and and Pakula, L.: Radiative-convective feedbacks in idealized states of radiative convective equilibrium, J. Atmos. Sci., 65, 3899–3916, 2008.
Storer, R. L. and van den Heever, S. C.: Microphysical Processes Evident in Aerosol Forcing of Tropical Deep Convective Clouds, J. Atmos. Sci., 70, 430–446, 2013.
Takahashi, H. and Luo, Z.: Where is the level of neutral buoyancy for deep convection?, Geophys. Res Lett., 39, L15809, doi:10.1029/2012GL052638, 2012.
Tompkins, A. M.: Organization of Tropical Convection in Low Vertical Wind Shears: The Role of Water Vapor, J. Atmos. Sci., 58, 529–545, 2001.
Tompkins, A. M. and Emanuel, K. A.: The vertical resolution sensitivity of simulated equilibrium temperature and water-vapour profiles, Q. J. Roy. Meteorol. Soc., 126, 1219–1238, 2000.
van den Heever, S. C., Stephens, G. L., and Wood, N. B.: Aerosol indirect effects on tropical convection characteristics under conditions of radiative-convective equilibrium, J. Atmos. Sci., 68, 699–718, 2011.
Walko, R. L., Cotton, W. R., Feingold, G., and Stevens, B.: Efficient computation of vapor and heat diffusion between hydrometeors in a numerical model, Atmos. Res., 53, 171–183, 2000.
Webster, P. J. and Lukas, R.: TOGA COARE. The Coupled Ocean–Atmosphere Response Experiment, Bull. Am. Meteorol. Soc., 73, 1377–1416, 1992.
Wexler, A.: Vapor Pressure Formulation for Ice, J. Res. Natl. Bur. Stand., 81A, 5–20, 1977.
Wood, R. and Field, P.R.: The Distribution of Cloud Horizontal Sizes, J. Climate, 24, 4800–4816, 2011.

Yuan, J. and Houze, R. A.: Deep Convective Systems Observed by A-Tain in the Tropical Indo-Pacific Region Affected by the MJO, J. Atmos. Sci., 70, 465–486, 2013.
Yuter, S. E. and Houze, R. A.: Three-Dimensional Kinematic and Microphysical Evolution of Florida Cumulonimbus, Part II: Distributions of Vertical Velocity, Reflectivity, and Differential Reflectivity, Mon. Weather Rev., 123, 1941–1963, 1995.
Yuter, S. E., Houze, R. A., Smith, E. A., Wilheit, T. T., and Zipser, E.: Physical characterization of tropical oceanic convection observed in KWAJEX, J. Appl. Meteor., 44, 385–415, 2005.
Zhang, C., Gottschalck, J., Maloney, E. D., Moncrieff, M. W., Vitart, F., Waliser, D. E., Wang, B., and Wheeler, M. C.: Cracking the MJO nut, Geophys. Res. Lett., 40, 1223–1230, doi:10.1002/grl.50244, 2013.
Zipser, E. J.: Mesoscale and Convective-Scale Downdrafts as Distinct Components of Squall-Line Structure, Mon. Weather Rev., 105, 1568–1589, 1977.

Table 1. Means of various length scales as a function of the number of cores. 3+ signifies that values are for cloud objects with 3 or more cores. The 25th and 75th percentile values are included in parentheses.

Cores	Pedestal Width (km)	Anvil Width (km)	Cutoff Height (km)	Anvil Depth (km)
1	11 (6, 13)	95 (33, 119)	7.2 (6.0, 8.3)	6.4 (5.3, 7.3)
2	20 (14, 25)	121 (50, 153)	7.3 (6.0, 8.4)	6.7 (5.7, 7.8)
3+	116 (42, 148)	335 (156, 449)	7.1 (6.0, 8.1)	7.7 (6.6, 8.8)

Table 2. Means of various length scales and number of cores as a function of binned pedestal width. The 25th and 75th percentile values are included in parentheses.

Pedestal Width (km)	Mean Pedestal Width (km)	Anvil Width (km)	Cutoff Height (km)	Anvil Depth (km)	Cores
< 25	14 (8.6, 18)	104 (39, 131)	7.2 (6.0, 8.3)	6.5 (5.4, 7.5)	1.6 (1, 2)
25–50	36 (30, 42)	175 (90, 217)	7.2 (6.1, 8.3)	7.2 (6.1, 8.2)	3.4 (3, 4)
> 50	156 (74, 193)	414 (228, 529)	7.0 (6.0, 8.1)	8.0 (6.9, 9.1)	10.9 (6, 13)

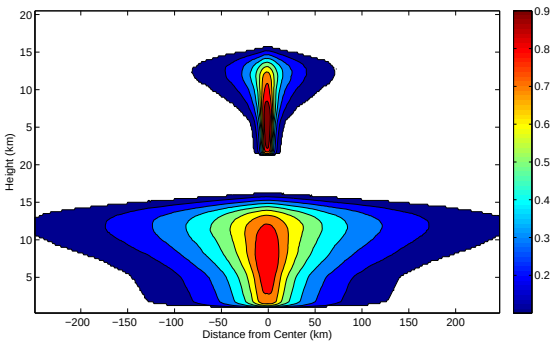

Figure 1. Overlap fraction for cloud objects of 1 (top), and 2 or more identified cores (bottom). The compositing method is detailed in IDV14.

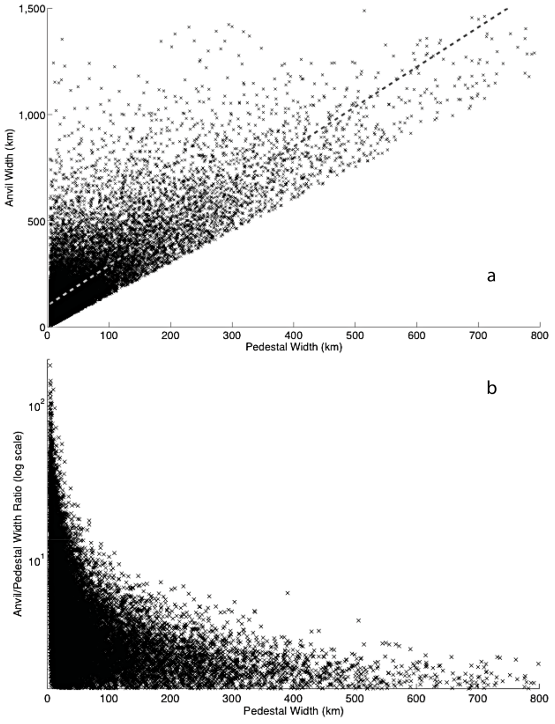

Figure 2. (a) Scatter plot of cloud object anvil and pedestal width pairs up to 1 500 and 800 km, respectively. The gray dashed line is a linear best fit to the data. The best fit has a slope of 1.9. 75 % of the population lies in low-valued pairs with pedestal widths less than 100 km and anvil widths less than 500 km. **(b)** Scatter plot of the ratios of anvil width to pedestal width.

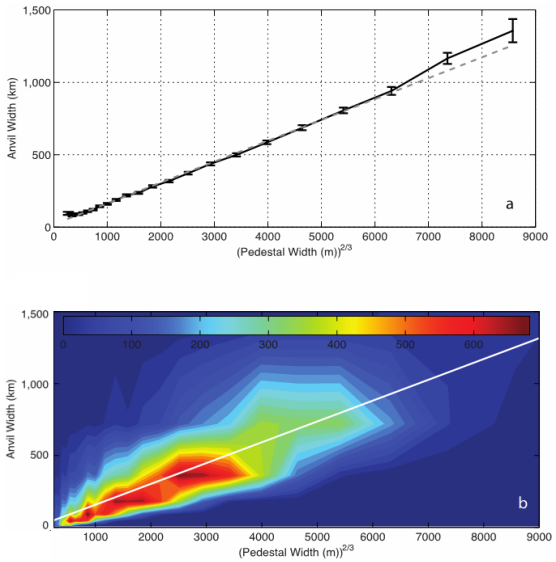

Figure 3. (a) The black solid line illustrates the mean anvil width binned by pedestal width. Error bars show the 95 % confidence interval for the mean. The gray dashed line shows the linear best fit to the data. **(b)** 2-D histogram of data binned by anvil width and pedestal width. The white line is the fit from **(a)**. Note that abscissa is pedestal width to the 2/3 power and in units of meters.

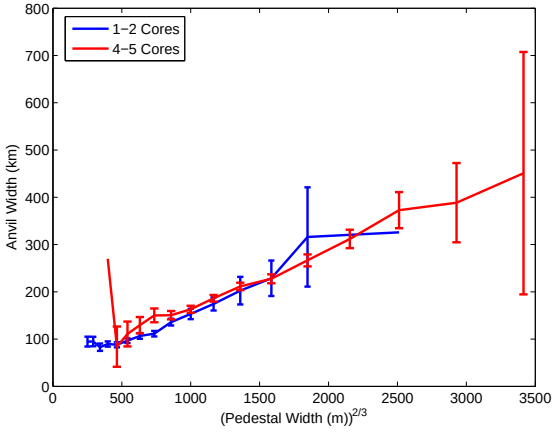

Figure 4. The blue data are for cloud objects with 1 to 2 identified cores. The red data are for those with 4–5 cores. Lines illustrates the mean anvil width binned by pedestal width. Error bars show the 95 % confidence interval for the mean.

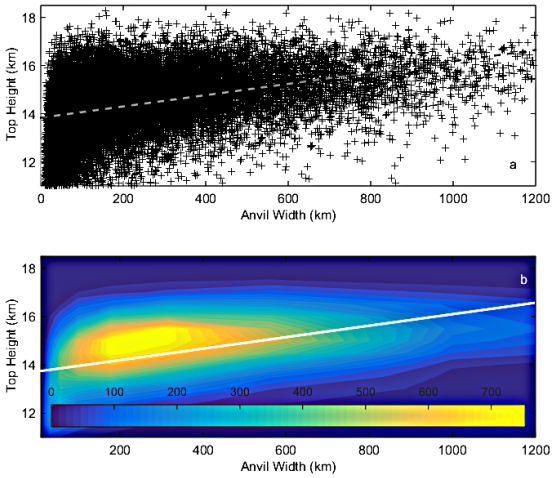

Figure 5. (a) A scatter of cloud object pairs of anvil width and top height with a linear least squares fit in the dashed line. **(b)** 2-D histogram of counts of data top heights and anvil widths bins with the same linear least squares fit as **(a)** in white. The data have been truncated to the region that exhibits frequent occurrences.

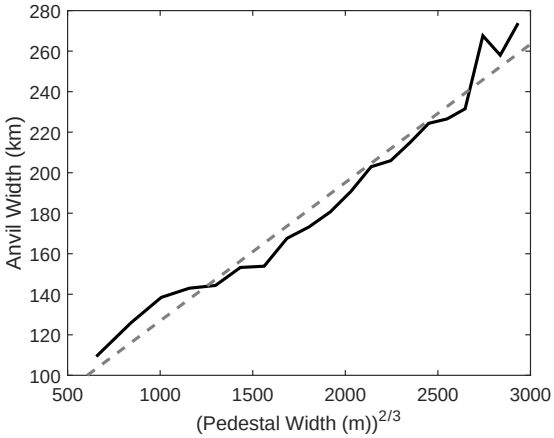

Figure 6. Mean anvil width as a function of binned pedestal with to the 2/3rd power in black. A linear fit is shown in the gray dashed line.

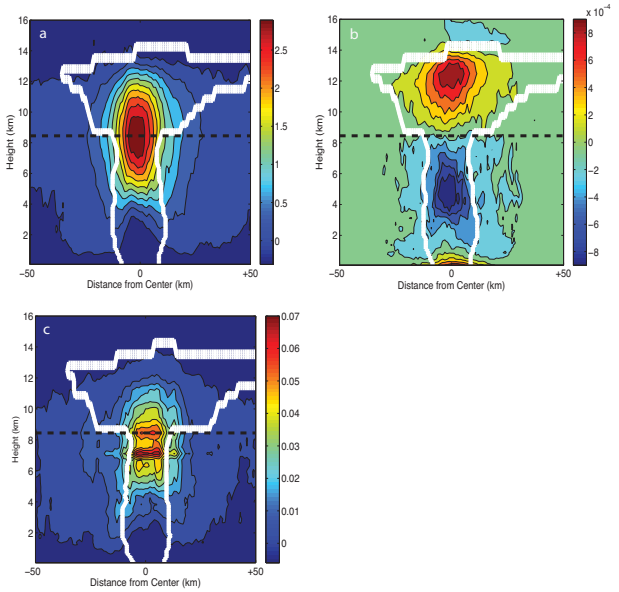

Figure 7. (a) composite of vertical velocities in colored contours, 50th percentile cloud outline in white, and mean anvil cutoff height in black dashes. **(b)** composite of mean horizontal divergence. **(c)** composite of mean depositional heating rates ($K\,h^{-1}$).

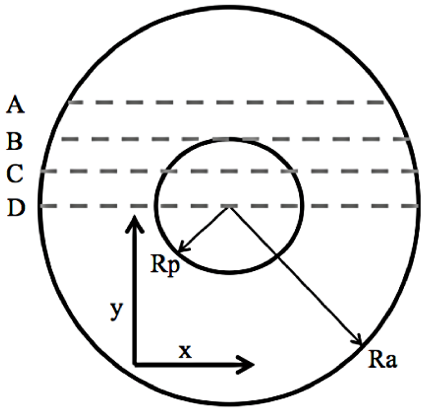

Figure A1. A potential plan view of a sampled cloud object with the outline of the convective pedestal and anvil in the thick, black circles. These have actual radii of R_p and R_a, respectively. Dashed, grey lines A–D are possible sampling tracks of CloudSat of this cloud object. Coordinates are labeled with the x axis along the sampling path.

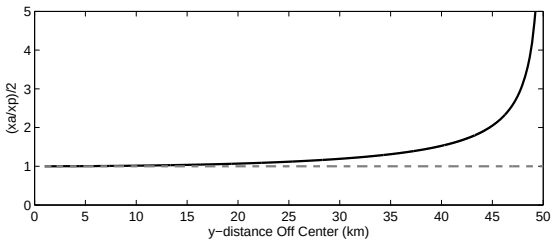

Figure A2. The factor by which off-center sampling affect a cloud object with R_a of 100 km and Rc of 50 km as a function of off-center distance.